



ORIGINAL ARTICLE

Antimicrobial air filter made of chitosan-ZnO nanoparticles immobilized on white silica gel beads



Muhammad Iqbal Hidayat^a, Muhammad Adlim^{a,b,*}, Suhartono Suhartono^c,
Zinatul Hayati^d, Noor Hana Hanif Abu Bakar^e

^a Graduate School of Mathematics and Applied Science, Universitas Syiah Kuala, Darussalam Banda Aceh 23111, Indonesia

^b Chemistry Department, FKIP, Universitas Syiah Kuala, Darussalam Banda Aceh 23111, Indonesia

^c Biology Department, Faculty of Mathematics and Natural Science, Universitas Syiah Kuala, Darussalam Banda Aceh 23111, Indonesia

^d Department of Microbiology, School of Medicine, Universitas Syiah Kuala, Banda Aceh, Indonesia

^e School of Chemical Sciences, Universiti Sains Malaysia, 11800 USM, Penang, Malaysia

Received 11 March 2023; accepted 26 April 2023

Available online 6 May 2023

KEYWORDS

Zinc oxide nanoparticles;
Immobilization;
Chitosan;
Silica gel beads;
Antibacterial properties;
Air filter

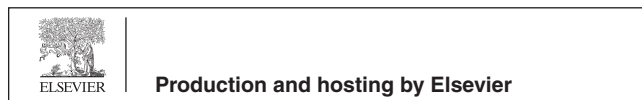
Abstract Airborne disease transmitted by biological air pollution threatens public space, therefore developing antimicrobial air filters is a crucial study. This study investigated the environmentally friendly preparation of synthetic zinc oxide nanoparticles ($\text{ZnO}_{\text{nano-synth}}$) at ambient temperature and the ZnO immobilization technique on silica gel beads coated with chitosan. The immobilized ZnO was used as an air filter in the simulated air chamber. Methanol swelled the 4.59 ± 0.5 wt % of the chitosan layer causing ZnO particles to stick to it, being stabilized, and dispersed. The dispersed ZnO particles of 5.18 ± 1.70 nm, thereby the efficacy preparation procedure is confirmed. The $\text{ZnO}_{\text{nano-synth}}$ exhibited high antibacterial properties against Gram-positive (*Staphylococcus aureus*) and Gram-negative (*Escherichia coli*) bacteria in agar media with inhibition diameters up to (33.50 ± 0.10) mm. Air filters containing the $\text{ZnO}_{\text{nano-synth}}$ -chi-SiG exhibited high and prolonged antibacterial activity against *Bacillus subtilis* in the air with 92% efficacy. These synthetic ZnO nanoparticles show better characteristics than commercial ZnO nanoparticles in terms of the particle size and the antibacterial properties of *Staphylococcus aureus* and *Escherichia coli*.

© 2023 The Author(s). Published by Elsevier B.V. on behalf of King Saud University. This is an open access article under the CC BY-NC-ND license (<http://creativecommons.org/licenses/by-nc-nd/4.0/>).

* Corresponding author at: Graduate School of Mathematics and Applied Science, Universitas Syiah Kuala, Darussalam Banda Aceh 23111, Indonesia.

E-mail addresses: adlim@unsyiah.ac.id, adlim@usk.ac.id (M. Adlim).

Peer review under responsibility of King Saud University. Production and hosting by Elsevier.



1. Introduction

Air quality has been the interest of study by researchers worldwide, due to the uncontrolled rise in population and human activities that have led to the emission of significant amounts of pollutants and bio-hazards into the environment. People spend about 16 h a day indoors and in working environments, which are mostly closed spaces (Vu et al., 2022). Hence the concern for environmental safety becomes a crucial issue. Among various tools and technologies such as mechanical collectors, electrostatic precipitators, and fabric filters; air purifiers are used to improve air quality indoors. Air purifiers are equipped with a High-Efficiency Particulate Air (HEPA) filter which is known to remove 99.97% of particles with a size of $\geq 0.3 \mu\text{m}$ diameter (Dubey et al., 2021; Zhang et al., 2022). Air purifiers with HEPA filters allow air to pass while capturing particles physically through four mechanisms (interception, inertial impaction, diffusion, and sieving). The smallest particles are removed by diffusion while the other three mechanisms work more effectively on large particles (Lowther et al., 2020). However, studies of air filter technologies for the elimination of bacteria and other microorganisms in the air are still rising (Li et al., 2018; Li et al., 2022; Watson et al., 2022).

The bacteria entrainment in indoor air can cause high risks of respiratory disease especially when the enclosed space has inadequate ventilation (Forthomme et al., 2014). In long periods with high relative humidity ($> 80\%$ room humidity), a proliferation of bacteria in the air that are subsequently stuck at the air filter can be hazardous even at low concentrations, especially for children (Harbizadeh et al., 2019). Thereby, antimicrobial air filter media is a crucial choice to reduce air-borne risk (Nunes et al., 2020).

The previous new design for antibacterial air filters loaded with silver nanoparticles (Ag NPs) (Hidayat et al., 2022; Cioritã et al., 2023; Ali et al., 2018), is still not cost-effective. This study focused on zinc oxide (ZnO) nanoparticles to substitute the silver nanoparticles. ZnO nanoparticles have several advantages including antibacterial and fungal properties (Gudkov et al., 2021; Ahmad et al., 2021; Decelis et al., 2017). The preparation and immobilization of ZnO nanoparticles on the solid support as a photocatalyst and potential air filter media have also been reported by our group (Muktardha et al., 2021). Zinc oxide/graphene immobilized on glass microfiber inactivated bacteria after ZnO was photochemically irradiated with a 60 Watt LED (Zhai et al., 2022). ZnO nanorods immobilized polytetrafluoroethylene (ePTFE) matrix were antibacterial air filters but reduced the filter's adequate porous size (Zhong et al., 2015). Nanofiber (ZnO@NF) hybrid membranes as air filters were fabricated by immobilized ZnO on PVA-co-PE nanofiber yarns (Yao et al., 2022). The antibacterial filter was prepared from polypropylene melt-blown nonwoven materials, in which ZnO was the electret material to absorb contaminants including bacteria (Han et al., 2022). When the filter fibers/cloth or membrane was coated permanently with ZnO then the air filter porosity becomes lessened, is easily fouled, and requires energy to pump in the air (Jatoi et al., 2019). Therefore, this current study altered the common ZnO preparation by immobilizing the ZnO nanoparticles on white silica gel beads to avoid airflow stuck, as part of newly designed effective and potentially reusable air filters. Low-cost and green preparation, immobilized and stable ZnO nanoparticles on the support are part of this study agenda. ZnO is usually synthesized involving sodium hydroxide and heating at a high temperature, while the preparation at room temperature as reported in this paper is still rare. The study continued with the antibacterial properties of the new environmentally friendly air filter design, providing possibilities for controlling pollutants indoors which are crucial in vulnerable places (De Almeida et al., 2022).

Green synthesized ZnO nanoparticles showed a strong bactericidal effect on a wide variety of pathogenic bacteria due to their biocompatibility, low toxicity, and high specific surface area (Huang et al., 2020; Amininezhad et al., 2014). Chitosan was used as a template for nanoparticle attachment, acted as a stabilizing agent, and prevent

the agglomeration of ZnO (Adlim et al., 2019), so the utilization of ZnO nanoparticles would be effective to apply as antibacterial air filters. Chitosan functioned as the stabilizer for metal nanoparticles is verified in the literature (Zarharan et al., 2023).

In this current study, the survival rates of *Staphylococcus aureus* and *Escherichia coli* bacteria which are typically Gram-positive and Gram-negative bacteria after contact with synthetic ZnO nanoparticles were investigated. *Staphylococcus aureus* and *Escherichia coli* themselves are pathogens, then their strains are pathogens. *Staphylococcus aureus* is notorious for causing skin and soft-tissue infections and it has the ability to infect nearly every organ system in the human body with often fatal consequences (Bose & Bayles, 2013). *Escherichia coli* is a foodborne pathogen that causes intestinal disease in humans (Govindarajan et al., 2020). The antibacterial filter experiment is only tested on gram-positive bacteria in the air since they were the dominant species producing flying spores in the air (Harbizadeh et al., 2019). Then *Bacillus subtilis* survival rates before and after penetration of the air filter chamber, are compared. These antibacterial performances provide possibilities for the future design of antibacterial air filters in consideration of their environmental friendliness, controlling pollutants indoors, when used correctly (with periodic maintenance) can provide better air quality in the environment (De Almeida et al., 2022).

2. Materials and method

2.1. Material

Chitosan of medium molecular weight ($\sim 400,000$) purchased from Sigma-Aldrich (CAS: 9012-76-4, USA; DD $> 75\%$), symbolized as 'chi-' and white silica gel beads (sorbed India production: spherical with specification refer to <https://www.silicagel-desiccant.com/silica-gel-white> (Desiccants, 2023) were purchased from the local market (Indonesia) and indicated as 'SiG'. Acetic acid glacial solution (CH_3COOH 98%), zinc nitrate hexahydrate crystal ($\text{Zn}(\text{NO}_3)_2 \cdot 6\text{H}_2\text{O}$), commercially available zinc oxide nanopowder (ZnO) denoted as $\text{ZnO}_{\text{nano-com}}$, and methanol (CH_3OH), and sodium hydroxide (NaOH) were of analytical grade and purchased from Merck KGaA (Indonesia). Distilled water (H_2O) was purchased from the Chemistry Laboratory of Syiah Kuala University (Indonesia). Bacteria of *Escherichia coli* (*E. coli*, ATCC 25922), *Staphylococcus aureus* (*S. aureus*, ATCC 25923), *Bacillus subtilis* (*B. subtilis*, ATCC 6633), Mueller-Hinton agar (MHA), and nutrient agar (NA) were all obtained from Dipa Puspa Labsains (Indonesia). All chemicals were used without further purification.

2.2. Equipment

A binocular microscope stereo (Olympus SZ61, Indonesia) equipped with an optical camera (OptiLab, Indonesia) was used to observe all samples including chi-SiG (original, before, and after immersing with several solvents), ZnO immobilized on chi-SiG, spore, and Gram staining. A scanning electron microscope (SEM, JEOL JSM 6360 LA, Indonesia) was used to observe the sample surface area. A transmission electron microscope (TEM, JEOL JEM-1400, Malaysia) was used to determine the particle size of ZnO. The zinc content on samples was analyzed with atomic absorption spectroscopy (AAS, ICE 3000 Series, Indonesia). Crystallinity analysis was carried out using X-ray diffraction (XRD, Shimadzu 7000, Indonesia). Spore and Gram staining were observed using a microscope (Olympus CX-21, Indonesia). Fourier-transform

infrared spectroscopy (FTIR, Shimadzu IR Prestige-21, Indonesia) was used to analyze the bonding of synthesized nanoparticles with functional groups of chitosan.

2.3. Procedure

2.3.1. Coating and characterization of chitosan on white silica gel beads

The coating procedure was prepared according to a previously described procedure (Adlim et al., 2021) with minor modifications. White silica gel beads (20.866 g) were soaked within 50 mL of chitosan solution for 60 min at room temperature, then it was dried in the oven for 60 min at 40 °C (called the first coating) and denoted as chi-SiG. Then, it was repeated to get the third coating. The drying process was carried out until a constant weight was obtained. The sample was characterized by using a binocular microscope stereo and SEM. The third coating chi-SiG was then used in the following experiments.

The coating stability of chi-SiG was verified by suspending the chi-SiG in several solvents. Several granules of chi-SiG were soaked into a separated small beaker with 5 mL of methanol, 5 mL of 0.1 M sodium hydroxide, and 5 mL of 1:1 (v/v) methanol-0.1 M sodium hydroxide for 60 min at room temperature. All chi-SiG was then dried in the oven for 60 min at 100 °C. The chi-SiG was observed using a binocular microscope stereo. The experiments were repeated for swelling studies but drying was excluded from the procedure. The different weights of dried and wet chi-SiG were recorded with an analytical balance (dried sample; W_0 and wet sample; W_1). The wet chi-SiG piece was air-dried and dried in the oven until the constant weight and denoted as W_2). The swelling studies were referred to in the previous study (Wu et al., 2018) with minor modifications.

The swelling property ($W_{sp}\%$) was calculated by using the equation:

$$W_{sp}\% = \frac{W_1 - M_0}{W_1} \times 100\% \quad (1)$$

Chitosan stability ($W_{cs}\%$) was calculated by using the equation:

$$W_{cs}\% = \frac{W_0 - M_2}{W_0} \times 100\% \quad (2)$$

$W_{sp}(\%)$ = swelling property

$W_{cs}(\%)$ = chitosan solubility

W_0 = weight of the dried sample before immersing it into the solvent

W_1 = weight of the wet sample after immersing into the solvent

W_2 = weight of the dried sample after immersing into the solvent

2.3.2. Immobilization and characterization of ZnO nanoparticles on chi-SiG

The synthesis of ZnO nanoparticles was prepared according to a previously described procedure (Donia et al., 2021; Haase et al., 1988) with some modifications and immobilized on chi-SiG. The chitosan layer on chi-SiG was used as the adhe-

sive and stabilizer for ZnO in the immobilization process. Crystal $\text{Zn}(\text{NO}_3)_2 \cdot 6\text{H}_2\text{O}$ (5.130 g) was dissolved in 10 mL methanol and transferred into a 100 mL flask. After all the crystals had been dissolved, 10 mL of 0.1 M NaOH was added, a cloudy white suspension was formed and then, the chi-SiG (30.140 g \sim 942 granules) was added into the flask. The flask was set in a rotary evaporator and rotated at 225 rpm, equipped with a water bath without heating. Furthermore, the Tungsten lamp (40 W at a 7 cm distance from the round flask) irradiated the round flask for 150 min and the temperature was maintained at \sim 40 °C. The sample was dried in the oven for 72 h at 60 °C and the color all changed to white. The sample is denoted as $\text{ZnO}_{\text{nano-synth}}\text{-[chi-SiG]}$. Two other samples were also prepared as a control. The first immobilization was ZnO nanopowder commercially available which was denoted as $\text{ZnO}_{\text{nano-com}}\text{-[chi-SiG]}$ and the second was $\text{Zn}(\text{NO}_3)_2$ symbolized as $\text{Zn}_{\text{salt}}\text{-[chi-SiG]}$ without the addition of NaOH. Immobilization of $\text{ZnO}_{\text{nano-com}}$ on chi-SiG was prepared by mixing wet chi-SiG (1.125 g) with 1.000 g of $\text{ZnO}_{\text{nano-com}}$ in a round flask and rotated with similar conditions as mentioned above before drying in the oven for 60 min at 60 °C. The samples were characterized with the light microscope, SEM, TEM, XRD, AAS, and FTIR methods.

The amount of zinc in all samples was calculated by using the AAS method. Each of $\text{ZnO}_{\text{nano-synth}}\text{-[chi-SiG]}$ (3.1628 g), $\text{ZnO}_{\text{nano-com}}\text{-[chi-SiG]}$ (3.0779 g), or $\text{Zn}_{\text{salt}}\text{-[chi-SiG]}$ (3.1272 g) was put into each 250 mL beaker and 5 mL of concentrated HNO_3 was added. The solution of each beaker was then mixed for 20 min by using a glass spatula. The distilled water (100 mL) was added and mixed thoroughly. The mixture was boiled until the volume was \sim 30 mL to expel nitric acid digestion gases and dissolve all soluble salts. The solution of each sample was filtered with a Whatman filter paper 2 into a 50 mL volumetric flask. The distilled water was added to each volumetric flask to rinse the filter paper up to 50 mL before the AAS analysis. Preparations of all zinc samples without SiG immobilization were repeated to prepare for XRD and antibacterial analysis.

2.3.3. The antibacterial property of $\text{ZnO}_{\text{nano-synth}}\text{-[chi-SiG]}$ against Gram-positive and Gram-negative bacteria

The antibacterial activity was performed by a previous study (Hidayat et al., 2021). All samples were tested against *S. aureus* and *E. coli* by determining the inhibition zone diameters after exposure to the sample. As a comparison, the use of SiG and chi-SiG as the control. The bacterial suspension was set to a 0.5 McFarland standard equal to 1.5×10^8 CFU/mL bacteria and inoculated on an agar plate of Mueller-Hinton agar (MHA). Three granules of each sample were put into a petri dish that contained MHA and bacterial suspensions. The agar was then incubated at 37 °C for 24 h before measuring the inhibition zone diameters. Screened the antibacterial activity of all samples, and then, the highest antibacterial activities were chosen to be applied in the simulated air filter. The research methodology flowchart is shown in Fig. 1.

2.3.4. Preparation of air filter chamber and air filter for the simulation

The air filter chamber was made of acrylic glass (34 cm \times 12 cm \times 11 cm) that was equipped with a small fan 5 V (8.8 cm \times 9 cm \times 3.7 cm) on the left side and another

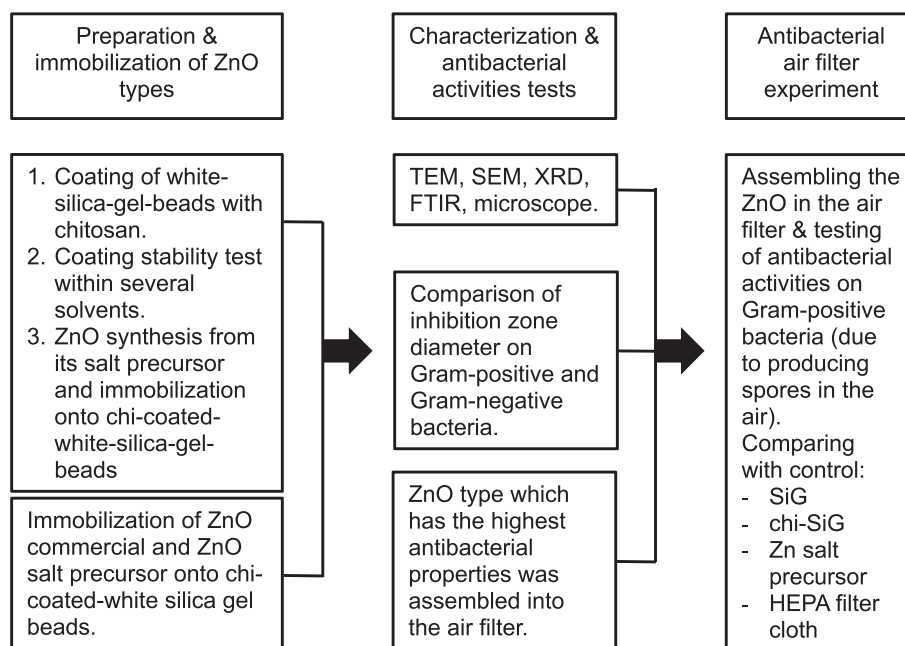


Fig. 1 The research methodology flowchart.

fan 12 V (10 cm × 10 cm × 2 cm) on the right side. Chamber was in the horizontal position. Two agar media were prepared; the first agar was contaminated with bacterial suspension of *B. subtilis* (on the left side) and another was a sterile agar media (on the right side) as presented in Fig. 2. The left fan was turned on to dry and flow media containing bacteria or spore, while the right fan was also turned on to blow the air out from the chamber. The air-containing bacteria was allowed to pass through the air filter. The experiment was performed for two days and both fans were run for 60 min per day at a velocity of 3.1 m/s. Bacteria colony before and after exposure was compared. Bacteria stuck on air filters was also observed. The detailed procedure for the antibacterial air filter test is described in Section 2.3.5. Furthermore, the air filter was made from pieces of nylon wire (10 cm × 10 cm) as presented in Fig. 3. This air filter has a pore size ± 1 mm to cover all granules in the filter. The prepared samples of $\text{ZnO}_{\text{nano-synth}}\text{-[chi-SiG]}$ were filled into the air filter to test. Air filters containing SiG, chi-SiG, $\text{Zn}_{\text{salt}}\text{-[chi-SiG]}$, and HEPA filter cloth (Sharp FZ-F30, Indonesia) were also prepared as the control for antibacterial testing. Each air filter was a single layer

containing ~ 629 granules. Furthermore, both the air filter chamber and filter were sterilized using UV light irradiation (ESCO airstream) at 250 nm for 30 min before the test run.

2.3.5. Antibacterial air filter containing $\text{ZnO}_{\text{nano-synth}}\text{-[chi-SiG]}$

A bacterial suspension of 1 McFarland standard that is equal to 3×10^8 CFU/mL bacteria was inoculated on an agar plate of nutrient agar and put into the air filter chamber. A single air filter containing $\text{ZnO}_{\text{nano-synth}}\text{-[chi-SiG]}$ was placed between *B. subtilis* agar and sterile agar media. The air filter chamber was incubated at 37 °C for 48 h and the air was flown in from *B. subtilis* agar media to penetrate the air filter containing $\text{ZnO}_{\text{nano-synth}}\text{-[chi-SiG]}$, and then the air was flown out from the chamber by a small fan. In the air filtration process, a small fan blew air slowly into the agar plate surface containing *B. subtilis* bacteria, and another fan drew air from the inside to get out from the air filter chamber. The agar plate was slowly dried and *B. subtilis* produced the spores (Setlow, 2006) which are rod-shaped and non-pathogenic bacteria present in low-temperature environments (Wightman et al., 2011; Headd &

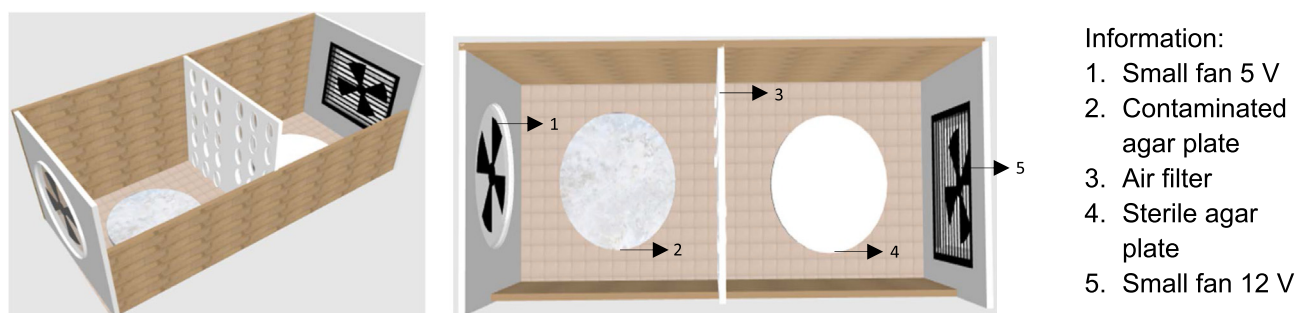


Fig. 2 Air filter chamber.

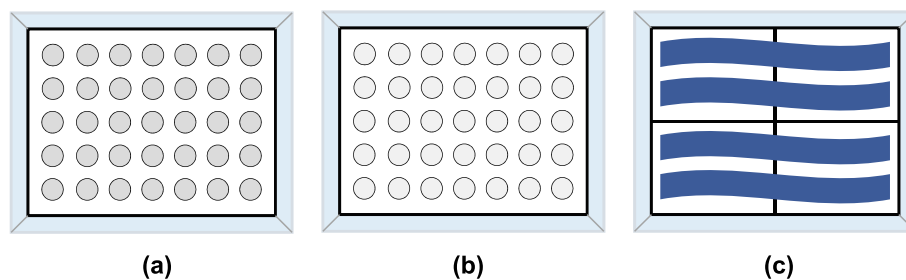


Fig. 3 Air filter containing (a) SiG, (b) $\text{ZnO}_{\text{nano-synth}}\text{-[chi-SiG]}$, and (c) HEPA filter.

Bradford, 2016). Air passed containing bacteria spores was flown into a sterile agar plate. The number of bacteria colonies before and after air filter penetration was investigated. The experiment was observed after 48 h incubation of the air filter chamber. Colonies were counted by using the colony counters (BISQUIT Industrial Co, Indonesia). A similar procedure was carried out for the air filter containing SiG, chi-SiG, $\text{Zn}_{\text{salt}}\text{-[chi-SiG]}$, HEPA filter cloth, and no filter (control) tested against *B. subtilis*. A comparison between total survival bacteria colonies detected passed through the filter with and without zinc content (control) was stated as the filter capacity for inactivating the bacteria or inactivation rate (%)

$$\begin{aligned} \text{Inactivation rate (\%)} \\ = \frac{(\Sigma \text{colonies in control} - \Sigma \text{survival colonies})}{\Sigma \text{colonies in control}} \times 100\% \end{aligned} \quad (3)$$

Furthermore, the bacteria staining procedure was conducted according to the Gram staining protocol (Gerhardt, 1980), and the spore staining procedure followed the Schaeffer-Fulton method using malachite green and safranin (Hussey & Zayaitz, 2007) toward air filter containing SiG and $\text{ZnO}_{\text{nano-synth}}\text{-[chi-SiG]}$ granules. Both Gram and spore staining were observed using a microscope.

3. Results and discussion

3.1. Coating and characterization of chitosan- $\text{ZnO}_{\text{nano-synth}}$ on SiG

Swelling properties and chitosan film covering the SiG in several solvents are analyzed from microscope images displayed in Table 1. Microscope images show that the chitosan layer was stable in methanol but dissolved or destroyed in a diluted sodium hydroxide solution. The image is consistent with Table 2 data showing that swelling in methanol caused less absorbed the solvent with W_{sp} of $4.59 \pm 0.5\%$ and without chitosan weight loss. In aqueous NaOH, however, most of the chitosan film disappears and then the SiG looks bald. Table 2 shows the swelling property was $24.45 \pm 1.0\%$ and $19.12 \pm 1.9\%$ of chitosan loss. The film breakage is due to deprotonating chitosan-acetic acid film that causes chitosan film loss from SiG. Chitosan dissolves in aqueous acetic acid by protonating the amino groups (Adlim et al., 2008). Others also found that chitosan-acetic acid solution precipitated in NaOH solution (Soon et al., 2018). The swelling moderately occurred in a mixture of methanol-diluted NaOH. The swelling was $23.35 \pm 3.5\%$ but only $4.49 \pm 0.3\%$ chitosan loss. Less chitosan loss in methanol-diluted NaOH might be due to

the low dissociation of hydroxide ions in methanol, causing a weaker deprotonating chitosan-acetic acid film. Unlike in water, NaOH dissolved slowly in methanol according to the previous report (PubChem, 2005). Moderate swelling is required to activate the adhesive property of chitosan film to attach ZnO without losing chitosan from the SiG support. Therefore, the last solvent formula is chosen for the following experiments.

Furthermore, chitosan film solubility was investigated from the swelling properties and presented in Table 2. Table 2 showed that all solvents caused the chitosan film to swell, but methanol performed the lowest swelling properties and sodium hydroxide was the highest. The result showed $4.59 \pm 0.5\%$, $24.45 \pm 1.0\%$, and $23.35 \pm 3.5\%$ for methanol, sodium hydroxide, and methanol-sodium hydroxide respectively. No chitosan dissolution occurred in methanol. Therefore, the mixture of methanol and sodium hydroxide is needed to minimize the swelling property that can lead to the dissolution of chitosan film on SiG. Our work showed that methanol-sodium hydroxide has lower chitosan solubility rather than sodium hydroxide only. Based on Table 2, chitosan film soluble in sodium hydroxide was $19.12 \pm 1.9\%$ while in methanol-sodium hydroxide was $4.49 \pm 0.3\%$, thus it proved to limit the excessive dissolution (weight loss) of chitosan film. Thereby, methanol-sodium hydroxide was chosen as the solvent for the immobilization of $\text{ZnO}_{\text{nano-synth}}$ onto chi-SiG.

$\text{ZnO}_{\text{nano-com}}$ which is commercially available was directly immobilized on chi-SiG and the synthetic ZnO was prepared from the nitrate salt and methanol-NaOH. The control and sample microscope images are presented in Fig. 4. $\text{ZnO}_{\text{nano-com}}$ was stuck directly on the chi-SiG so that $\text{ZnO}_{\text{nano-com}}$ covered almost all SiG surfaces as shown in Fig. 4(a) which is a different appearance from synthetic ZnO (Fig. 4b) and chi-SiG as control (Fig. 4c).

Based on the Sigma Aldrich database, the Zn precursor price and the preparation cost of ZnO nanoparticles have a lower price than gold and silver nanoparticles and are comparable with the commercial ZnO nanoparticles, which all have antibacterial properties (Sigma Aldrich, 2023a,b,c; Bankar et al., 2020; Ahmad et al., 2021). Immobilization of synthetic ZnO on chi-SiG involves several steps. It initiates Zn(OH)_2 formation and conversion of Zn(OH)_2 into ZnO after the heating process. Heating was at a moderate temperature (60°C) to avoid chitosan film burning since chitosan starts decomposing significantly at 230°C (Muktariidha et al., 2022). Formation of ZnO at low temperatures has been recently known but the zinc precursors were mostly not zinc nitrate (Tadji et al., 2022). Also, previous literature confirmed that ZnO formation had been proven in an alcoholic solution containing a small

Table 1 Observation result of chi-SiG immersion in several solvents through binocular microscope stereo with 15 × magnification.

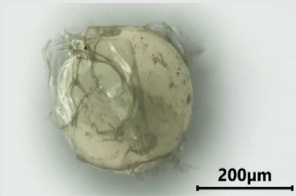
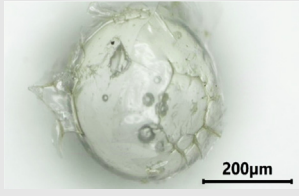
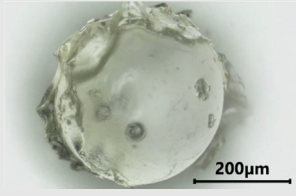
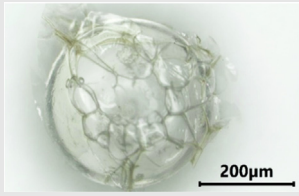
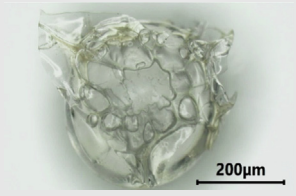
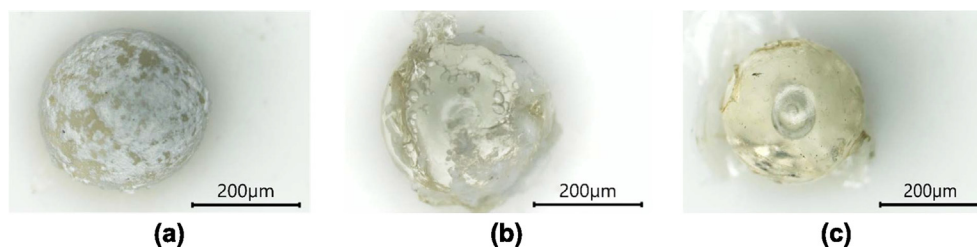
Solvent	Before immersion	After immersion
Methanol		
Sodium hydroxide 0.1 M		
Methanol-sodium hydroxide 0.1 M		

Table 2 The result of swelling property and chitosan solubility in several solvents using a gravimetric method.

Solvent	No.	W_0 (g)	W_1 (g)	W_2 (g)	W_{sp} (%)	W_{cs} (%)
Methanol	1	0.046	0.048	0.046	4.16	0
	2	0.044	0.047	0.044	4.48	0
	3	0.039	0.041	0.039	5.13	0
mean ± SD					4.59 ± 0.5	0
Sodium hydroxide 0.1 M	1	0.059	0.077	0.049	23.37	16.95
	2	0.050	0.067	0.040	25.37	20.00
	3	0.049	0.065	0.039	24.61	20.41
mean ± SD					24.45 ± 1.0	19.12 ± 1.9
Methanol-sodium hydroxide 0.1 M	1	0.073	0.091	0.070	19.78	4.11
	2	0.065	0.085	0.062	23.53	4.61
	3	0.063	0.086	0.060	26.74	4.76
mean ± SD					23.35 ± 3.5	4.49 ± 0.3

W_o = dried sample weight, W_l = wet sample weight after immersion,

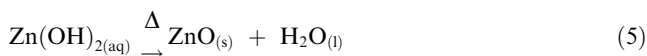
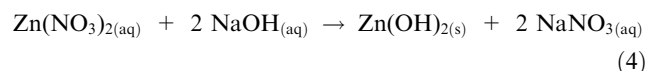
W_2 = dried sample weight after immersion, W_{sp} = swelling property, W_{cs} = weight chitosan loss.

**Fig. 4** Cross-section image of (a) $ZnO_{nano-com}$ -[chi-SiG], (b) $ZnO_{nano-synth}$ -[chi-SiG], and (c) chi-SiG through binocular microscope stereo with 15 × magnification.

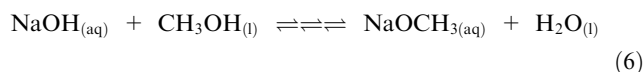
amount of water, and the process involved a complex mechanism (Haase et al., 1988).

The surface and shape studies of the synthesized nanoparticles were carried out by optical microscope and SEM. Microscope images revealed that chitosan film covered the entire chi-SiG (Fig. 4a) as proven by the yellowish transparent color and allowed the attachment of the ZnO_{nano-synth} (Fig. 4b) and ZnO_{nano-com} (Fig. 4c) as confirmed by the white color on the chi-SiG surface. A closer appearance of chitosan film and ZnO_{nano-synth} observed in SEM image showed the chitosan film has smooth layers and its microfibril covered the entire surface of SiG (indicated by the yellow line in Fig. 5a). At higher magnification (5000 x), some spherical and sheet-like shaped existed (Fig. 5b). The presence of chitosan film on SiG provides sites for ZnO and it prevents ZnO from agglomeration. The different appearance observed on ZnO_{nano-com} images confirmed agglomerated nanopowder, with larger particle size and chitosan film was not obvious (Fig. 5c). According to AAS data, the zinc weight in each granule sample of ZnO_{nano-synth}-[chi-SiG] and ZnO_{nano-com}-[chi-SiG] was 0.304 mg and 0.498 mg, respectively.

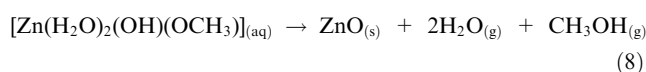
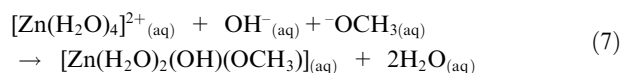
The synthesis of ZnO_{nano-synth}-[chi-SiG] involves a two-stage process, i.e., hydroxylation and drying. In the present paper, the reaction temperature was carried out at ~ 40 °C and the drying temperature at a low degree (60 °C). In this work, the drying temperature plays a role in the formation of ZnO, as it allows the dehydration of residual Zn(OH)₂ to form ZnO. According to Biron et al (2020), the syntheses follow the reaction step:



Another possible reaction of the interaction between NaOH, methanol, water, and zinc salt is the involvement of methoxide ion (-OCH₃) as the reaction product NaOH and CH₃OH. Although the reaction is in equilibrium with small *K*, during slow heating, the water evaporated and the equilibrium goes to the right side, thereby the methoxide ion might exist. The proposed reaction has been previously published (Xiong et al., 2014). NaOCH₃ then dissociates into sodium and methoxide ions.



According to Crystal Field Theory, zinc ions in the water will be surrounded by four H₂O molecules, which is a common coordination number for Zn complexes. Then, the H₂O molecules are replaced by hydroxyl and methoxide (-OCH₃) ligands as the proposed reaction:



The comparative FTIR spectra of unmodified chitosan and chitosan-ZnO_{nano-synth} were depicted and studied (shown in Fig. 6). The specific absorption peaks of the original chitosan were observed at 3420 cm⁻¹ (NH₂ and OH stretching vibrations), 2944 cm⁻¹ and 2881 cm⁻¹ (asymmetric and symmetric stretching vibrations of -CH₂ groups), 1640 cm⁻¹ and 1579 cm⁻¹ (C-O stretching vibration of amide I and -NH₂ bending vibration of amide II) which are consistent with previously reported work (Sarjini et al., 2019; Kumar et al., 2019; Sun et al., 2020). In the chitosan-ZnO_{nano-synth} spectra, compared with chitosan, the broader and stronger peak moved

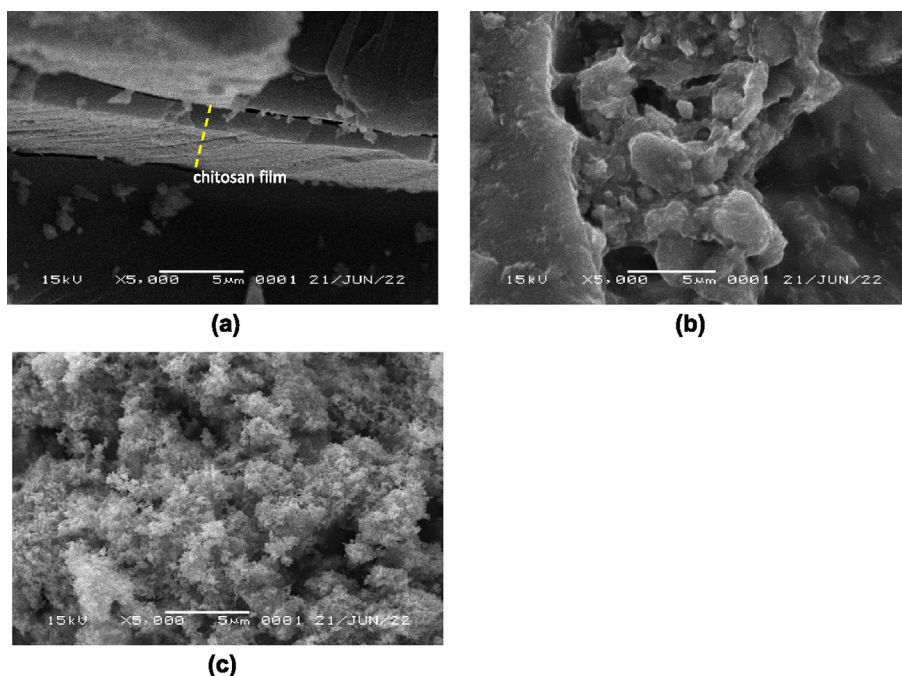


Fig. 5 SEM images of (a) chi-SiG, (b) ZnO_{nano-synth}-[chi-SiG], and (c) ZnO_{nano-com}-[chi-SiG] with 5000 × magnification.

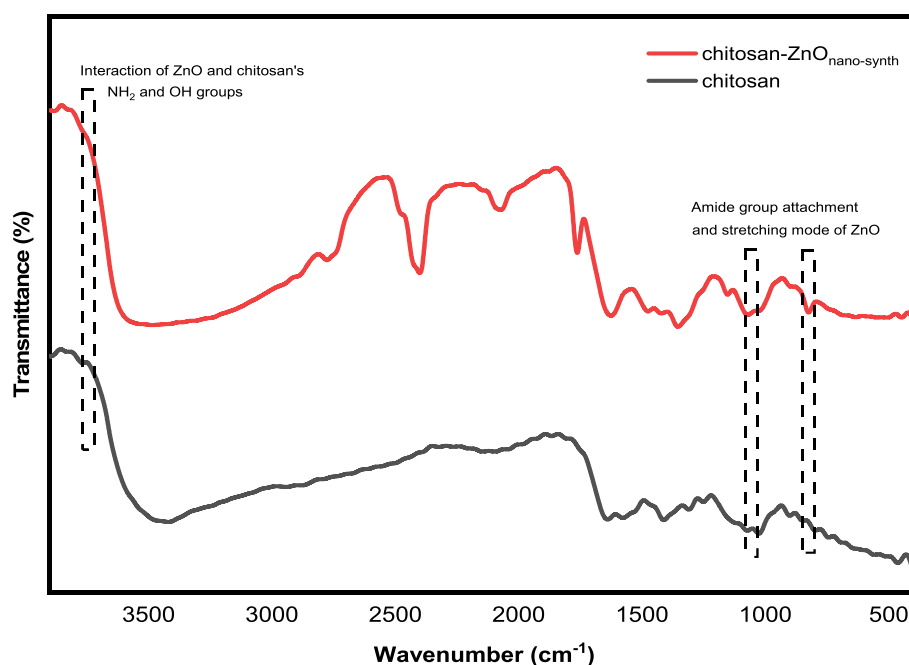
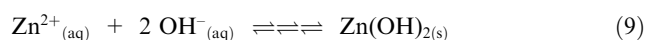


Fig. 6 FTIR spectra of chitosan and chitosan-ZnO_{nano-synth}.

noticeably to wavenumber at 3486 cm^{-1} which indicated the interaction between ZnO molecules and chitosan's NH_2 and OH groups (Balogun et al., 2020). In addition, the absorption peaks formed at 675 cm^{-1} and 449 cm^{-1} are due to the attachment of the amide group and stretching mode of ZnO, respectively (Balogun et al., 2020; Vijayalakshmi et al., 2015). Thus, a broader and stronger peak in chitosan-ZnO hypothesizes the weak chemical interaction between ZnO molecules and the binding sites of chitosan.

When chitosan and zinc oxide dissolved; thereby; regulating the acidity of the solution, Zn^{2+} ions were formed. At $\text{pH} = 6-9$ the unstable compound $\text{Zn}(\text{OH})_2$ was formed, according to the following equation:



Chitosan's NH_2 and OH groups can form coordination bonds with metal ions (Ardean et al., 2021), by increasing the pH of the solution to $\text{pH} = 10$ dropwise addition of NaOH, the stable complex of chitosan-ZnO_{nano-synth} is formed. In this work, chitosan may have played a major role in stabilizing zinc oxide nanoparticles.

The size and distribution of ZnO were analyzed using TEM images of ZnO_{nano-synth}-[chi-SiG] and ZnO_{nano-com}-[chi-SiG]. The solid samples were immersed in water and the slurry was analyzed with TEM methods. The particle size distribution was calculated from around 300 particles with diameter calculated using software of image-J, where the data were presented as mean \pm standard deviation (SD) (Aljabali et al., 2018) as tabulated in Fig. 7 and Fig. 8. The TEM images of ZnO_{nano-synth} exhibited well-dispersed spherical shapes with an average particle size of $5.18 \pm 1.70\text{ nm}$. The presence of chitosan as a stabilizer prevents particles from agglomeration (Ranjani et al., 2019). However, ZnO_{nano-com} was aggregated with a sheet-like shape and an average particle size of $30.83 \pm 0.75\text{ nm}$. The particles were not dispersed well and had

smaller size deviations. The different distribution of ZnO onto the chi-SiG surface has a relation to the immobilization technique; ZnO_{nano-synth}-[chi-SiG] was synthesized from the salt, while ZnO_{nano-com}-[chi-SiG] was directly used from the nanopowder. The appropriate immobilization technique causes the ZnO surface to be assessable for bacteria to contact. This finding was verified in the previous study of the immobilization of chi-Pd/Au on titania (Adlim & Bakar, 2013) and the immobilization of Ag NPs on chi-pumice (Adlim et al., 2021). Therefore, this promising-immobilization technique was confirmed as an appropriate method with several advantages including being environmentally friendly, low energy, not toxic, and low cost.

Analysis was conducted to compare the crystallinity and impurity of the ZnO_{nano-synth}-[chi-SiG] with ZnO_{nano-com}-[chi-SiG]. The XRD measurement was performed at room temperature with an X-ray, continuous scan (2θ) in the range of 10 to 70° with a 0.02 -degree step. The diffraction patterns are matched with the ZnO standard diffractogram (marked by the \bullet ; JCPDS: 036-1451) as a wurtzite structure and no characteristic peaks were observed other than ZnO. Miller indices marked by the \bullet ; (100), (002), (101), (102), (110), (103), and (200) from left to right (Bindu & Thomas, 2014). The diffractogram shows that ZnO_{nano-synth}-[chi-SiG] (ZnO synthesized at 60°C) has low crystallinity as shown in Fig. 9. In contrast, the synthesized ZnO_{nano-synth} at 150°C exhibits seven diffraction peaks located at 31.7 , 34.4 , 36.2 , 47.5 , 56.5 , 62.8 , and 67.9° . These peaks are indexed as the spherical to the hexagonal phase of ZnO with high crystallinity of the particles (Khoshhesab et al., 2011; Faisal et al., 2021). It was revealed that all of the characteristic peaks were of ZnO_{nano-synth} and no such impurities exist in the ZnO_{nano-synth}.

The diameter of ZnO crystallites was calculated by the Debye-Scherrer formula, on the bases of θ (Bragg's diffraction angle) and β (full width at half maximum (FWHM)) of the most intense peaks corresponding to the (101) planes located

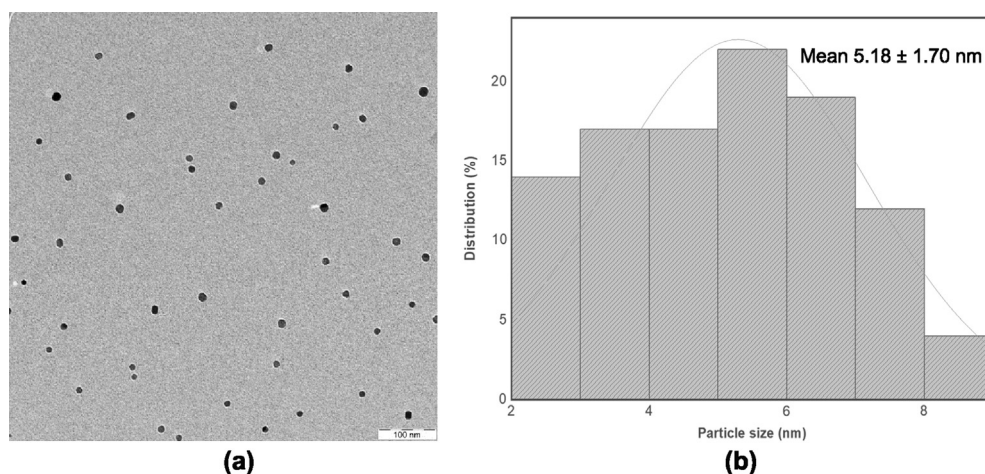


Fig. 7 TEM analysis of (a) $\text{ZnO}_{\text{nano-synth}}$ from $\text{ZnO}_{\text{nano-synth}}\text{-[chi-SiG]}$ (scale bar 100 nm), and (b) particle size distribution.

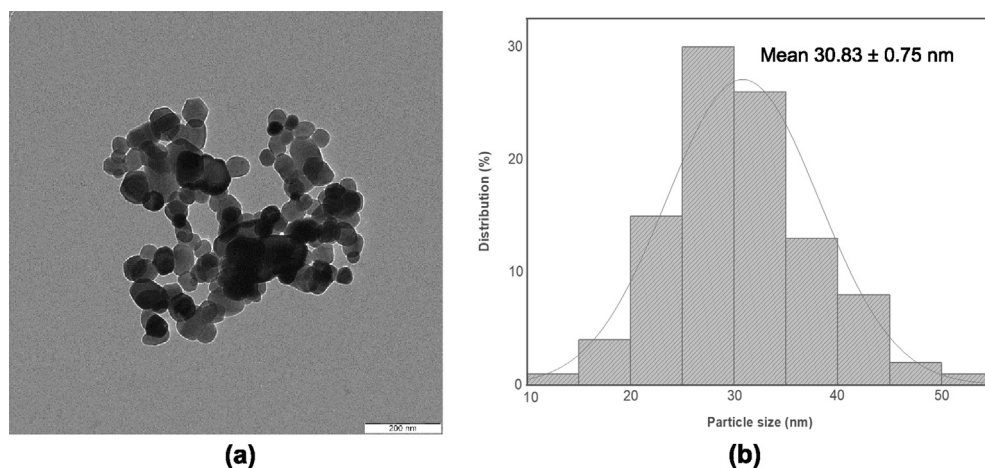


Fig. 8 TEM analysis of (a) $\text{ZnO}_{\text{nano-com}}$ from $\text{ZnO}_{\text{nano-com}}\text{-[chi-SiG]}$ (scale bar 200 nm), and (b) particle size distribution.

at approximately 36.2° . The crystallite size is about 31.9 nm for $\text{ZnO}_{\text{nano-synth}}$ (synthesized at 150°C) while the crystallite size is about 23.1 nm for $\text{ZnO}_{\text{nano-com}}$ as presented in detail in Table 3. The indexation confirms the standard hexagonal wurtzite structure (JCPDS: 036–1451) of $\text{ZnO}_{\text{nano-synth}}$ as previously reported in other studies (Arakha et al., 2015). ZnO crystallizes in the wurtzite structure in which the oxygen atoms are arranged in a hexagonal close-packed type with zinc atoms occupying half the tetrahedral sites (Bindu & Thomas, 2014). Zn and O atoms are tetrahedrally coordinated with each other and have, therefore, an equivalent position.

The comparison of lattice parameters between $\text{ZnO}_{\text{nano-synth}}$ (synthesized at 150°C) and $\text{ZnO}_{\text{nano-com}}$ are listed in Table 4. The a and b are equivalent to wurtzite crystallite dimension and c is much larger. The (100) plane was used to determine a and b, while the (002) plane determine c (Bindu & Thomas, 2014). The ratio of c/a, bond length, the volume of the unit cell, and atomic packing factor (APF) are all matched with the ZnO standard (JCPDS: 036–1451). The APF of ideal hexagonal ZnO is 74% (Kanchana et al., 2016) and it was found about 75.5%, which means that the APF

of nanocrystals is slightly more than that of bulk materials. It may be due to the size effect in nanocrystalline powders. Furthermore, all the lattice parameters are well-matched with the ZnO standard of the JCPDS.

3.2. Antibacterial study for ZnO without immobilization sample

Antibacterial activities were tested for several samples that were ZnO without immobilization, the $\text{ZnO}_{\text{nano-synth}}\text{-[chi-SiG]}$, and the air filter containing $\text{ZnO}_{\text{nano-synth}}\text{-[chi-SiG]}$. The antimicrobial properties are compared among $\text{ZnO}_{\text{nano-synth}}$ synthesis at 60°C and 150°C , and $\text{ZnO}_{\text{nano-com}}$. The antibacterial data for ZnO without immobilization are presented in Table 5. All samples exhibit an inhibition zone against *S. aureus* and *E. coli* as shown in Fig. 10. $\text{ZnO}_{\text{nano-synth}}$ synthesized at 60°C has less crystalline characteristic according to XRD data but it shows the highest antibacterial activity against both types of bacteria with an inhibition zone diameter of 33.50 ± 0.10 mm (*S. aureus*) and 30.08 ± 0.03 mm (*E. coli*). The $\text{ZnO}_{\text{nano-synth}}$ synthesized at 150°C also exhibit a moderate inhibition zone against *S. aureus* and *E. coli* with a

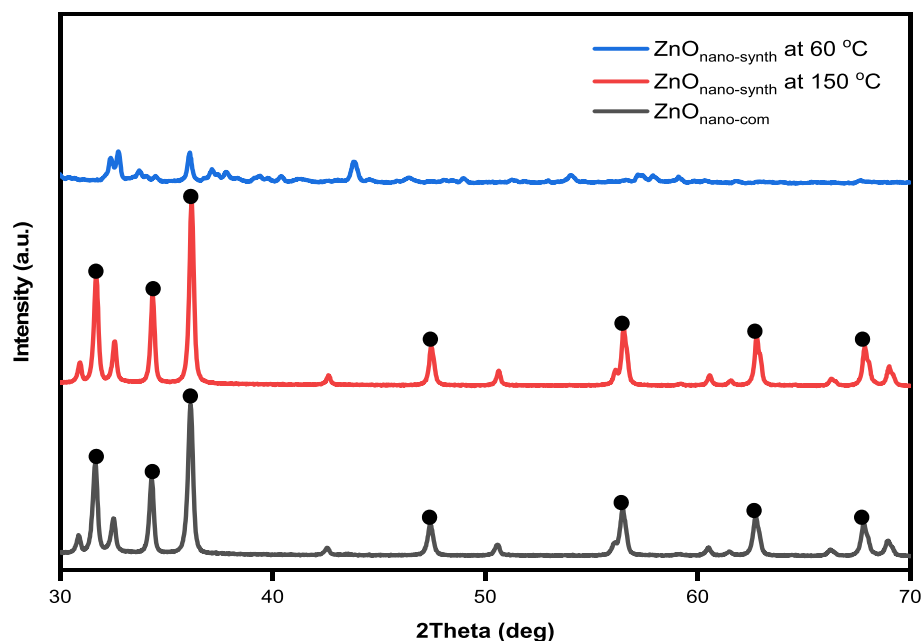


Fig. 9 Diffraction of $\text{ZnO}_{\text{nano-synth}}$ (at 60 °C and 150 °C) and $\text{ZnO}_{\text{nano-com}}$.

Table 3 Detail of crystallite and particle size.

Plane	Diffraction angle $\text{ZnO}_{\text{nano-synth}}$	Diffraction angle $\text{ZnO}_{\text{nano-com}}$	Crystallite size 'D' (nm)	
			$\text{ZnO}_{\text{nano-synth}}$	$\text{ZnO}_{\text{nano-com}}$
(100)	31.7	31.7	30.3	27.5
(002)	34.4	34.3	33.4	30.9
(101)	36.2	36.1	31.9	23.1
(102)	47.5	47.4	31.9	27.9
(110)	56.5	56.5	31.2	26.6
(103)	62.8	62.7	30.2	25.3
(200)	67.9	67.8	28.2	24.1

Table 4 The crystal parameter of $\text{ZnO}_{\text{nano-synth}}$ and $\text{ZnO}_{\text{nano-com}}$.

Sample	d_{hkl}		Lattice constant		(c/a)	Bond length 'L' (Å)	The volume of the unit cell 'V'	Atomic packing factor 'APF' (%)
	1 0 0	0 0 2	a (Å)	c (Å)				
$\text{ZnO}_{\text{nano-synth}}$	2.8	2.6	3.3	5.2	1.6	1.9	47.9	75.5
$\text{ZnO}_{\text{nano-com}}$	2.8	2.6	3.3	5.2	1.6	1.9	48.1	75.5
ZnO-JCPDS	2.8	2.6	3.3	5.2	1.6	1.9	47.6	75.5

diameter zone of 27.62 ± 0.08 mm and 22.49 ± 0.11 mm, respectively. $\text{ZnO}_{\text{nano-com}}$ shows the lowest antibacterial activity against *S. aureus* with 6.26 ± 0.15 mm inhibition zone diameter, although according to AAS data, $\text{ZnO}_{\text{nano-com}}$ has higher zinc content compared to synthetic $\text{ZnO}_{\text{nano-synth}}$.

Furthermore, the finding suggested that $\text{ZnO}_{\text{nano-synth}}$ had a stronger antibacterial effect on Gram-positive (*S. aureus*) than on Gram-negative (*E. coli*) bacteria due to their different cell wall components. The Gram-negative (*E. coli*) bacteria have multilayer structures of cell walls containing peptidoglycan layer, lipoprotein layer, phospholipids, or lipopolysaccharide layer (Siripatrawan & Vitchayakitti, 2016). These complex layer structures caused weaker interaction between ZnO and

cells if it is compared to the Gram-positive cell wall properties. Since the $\text{ZnO}_{\text{nano-synth}}$ synthesized at 60 °C has stronger antibacterial then this sample was involved in further study of antibacterial tests for the $\text{ZnO}_{\text{nano-synth}}$ immobilization and the antibacterial air filter samples.

3.3. Antibacterial study for ZnO immobilized on chi-SiG sample

After samples of ZnO without immobilization on chi-SiG showed high antibacterial characteristics, then study the immobilized ZnO samples because they were prepared differently. The $\text{ZnO}_{\text{nano-synth}}$ -[chi-SiG] granules were evaluated for their antibacterial properties before being assembled as the

Table 5 Inhibition zone diameter of several ZnO without immobilization on chi-SiG.

Bacteria	Sample codes of ZnO without immobilization on chi-SiG	Inhibition zone diameters (mm) (mean \pm SD)
<i>Staphylococcus aureus</i>	ZnO _{nano-com}	6.26 \pm 0.15
	ZnO _{nano-synth} synthesized at 60 °C	33.50 \pm 0.10
	ZnO _{nano-synth} synthesized at 150 °C	27.62 \pm 0.08
<i>Escherichia coli</i>	ZnO _{nano-com}	0
	ZnO _{nano-synth} synthesized at 60 °C	30.08 \pm 0.03
	ZnO _{nano-synth} synthesized at 150 °C	22.49 \pm 0.11

All experiments were performed in triplicates and reported as mean \pm standard deviation (SD).

Table 6 Inhibition zone diameter of prepared samples.

Bacteria	Sample codes	Inhibition zone diameters (mm) (mean \pm SD)
<i>Staphylococcus aureus</i>	SiG	0
	chi-SiG	13.06 \pm 0.11
	Zn _{salt} -[chi-SiG]	32.05 \pm 0.03
	ZnO _{nano-synth} -[chi-SiG]	33.33 \pm 0.07
	ZnO _{nano-com} -[chi-SiG]	20.28 \pm 0.98
<i>Escherichia coli</i>	SiG	0
	chi-SiG	15.29 \pm 0.38
	Zn _{salt} -[chi-SiG]	28.41 \pm 0.26
	ZnO _{nano-synth} -[chi-SiG]	29.54 \pm 0.33
	ZnO _{nano-com} -[chi-SiG]	18.43 \pm 0.84

air filter. The characteristics of synthetics ZnO_{nano-synth}-[chi-SiG] (prepared at 60 °C) were compared with some of the control sample properties including SiG, chi-SiG, Zn_{salt}-[chi-SiG], and ZnO_{nano-com}-[chi-SiG], based on the inhibition zone diameter. As presented in Table 6 that all samples exhibited the inhibition zone against *S. aureus* and *E. coli* except SiG. The chi-SiG displayed antibacterial activity with an inhibition zone diameter of 13.06 \pm 0.11 mm (*S. aureus*) and 15.29 \pm 0.38 mm (*E. coli*). Similarly, other samples such as ZnO_{nano-com}-[chi-SiG], Zn_{salt}-[chi-SiG], and ZnO_{nano-com}-[chi-SiG] exhibited the antibacterial properties against both types of bacteria (shown in Fig. 11), this indicated that zinc ions and zinc oxide nanoparticles act as antibacterial agents, but the ZnO_{nano-synth}-[chi-SiG] performed the strongest. The inhibition zone diameter of ZnO_{nano-synth}-[chi-SiG] against *S. aureus* and *E. coli* was 33.33 \pm 0.07 mm and 29.54 \pm 0.33 mm, respectively. These indicated that ZnO particles along with chitosan inhibit bacterial growth by diffusion of the soluble species into the agar medium.

Chitosan is effective against a wide range of target organisms and is available in a variety of formulations including

films (Costa-Pinto et al., 2021) as shown in chi-SiG. However, chitosan only has weak antibacterial without combining with ZnO. The suggested mechanisms of action are based on the electrostatic interaction between chitosan positively charged amino groups and the predominantly anionic lipopolysaccharide on Gram-negative bacteria or teichoic acid on Gram-positive bacteria (Kulawik et al., 2020). In Gram-positive bacteria, chitosan interacted with lipopolysaccharide molecules and displaced divalent cations within bacteria cells (e.g., Ca²⁺ and Mg²⁺) inducing depolarization of the cell membrane, leading to increased permeability, osmotic damage, intercellular leakage and ultimately cell death. In Gram-negative bacteria, chitosan diffused inside the cell bonded to the cellular membrane and inhibited their growth (Duan et al., 2019).

Zinc ions are involved in the regulation of cell growth and differentiation of the membrane structure of bacterial cells (Jafarirad et al., 2016), for example in Zn_{salt}-[chi-SiG] granules, an excess of Zn²⁺ may compete with other metals and

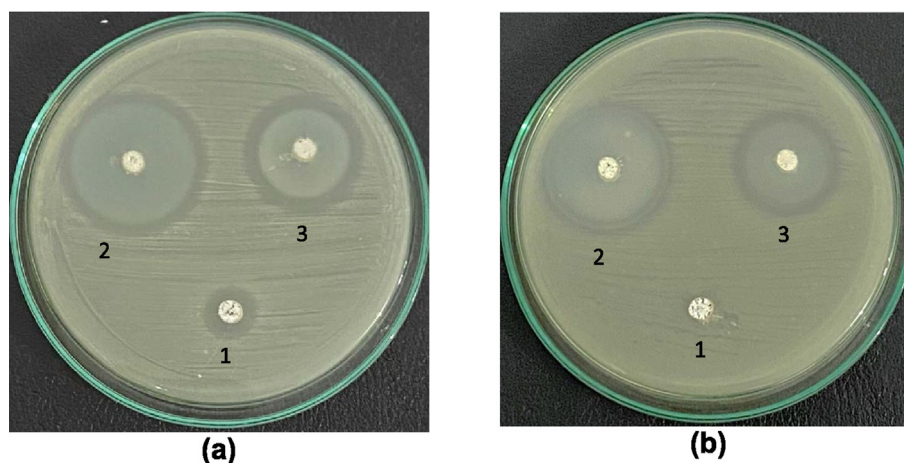


Fig. 10 Antibacterial activity against (a) *S. aureus* and (b) *E. coli*; (1) ZnO_{nano-com}, (2) ZnO_{nano-synth} synthesized at 60 °C, and (3) ZnO_{nano-synth} synthesized at 150 °C.

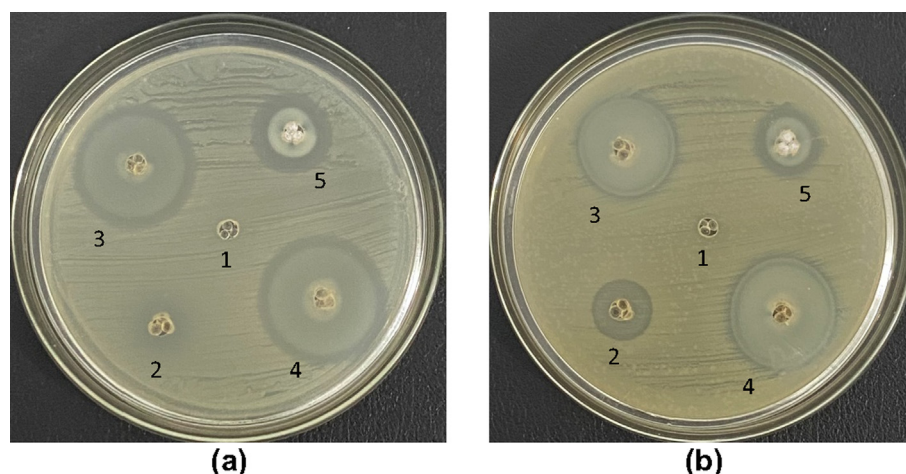


Fig. 11 Antibacterial activity against (a) *S. aureus* and (b) *E. coli*; (1) SiG, (2) chi-SiG, (3) $\text{Zn}_{\text{salt}}\text{-[chi-SiG]}$, (4) $\text{ZnO}_{\text{nano-synth}}\text{-[chi-SiG]}$, and (5) $\text{ZnO}_{\text{nano-com}}\text{-[chi-SiG]}$.

provoke a metal mismatch in various metal-binding proteins resulting in protein malnutrition, enzymatic inactivation, or protein denaturation, thus leading to the bacterial cell off balance (Godoy-Gallardo et al., 2021). However immobilized zinc salt (representing Zn^{2+} sample) without converting into ZnO , will easily leach from the chi-SiG support in a humid environment thereby it might be not long-lasting and not easily regenerated for reusable.

The toxicity mechanism mediated by zinc oxide nanoparticles, in $\text{ZnO}_{\text{nano-synth}}\text{-[chi-SiG]}$, is mainly linked to the release of Zn^{2+} ions (Deng et al., 2009) and attributed to the nanoparticles themselves (Yang et al., 2009). The proposed mechanisms are listed as follows: (1) loss of cellular integrity by direct contact of $\text{ZnO}_{\text{nano-synth}}$ with the cell wall and/or membrane and (2) release of Zn^{2+} ions upon $\text{ZnO}_{\text{nano-synth}}$ dissolution and followed by intercellular reactive oxygen species (ROS) production subsequent and damage of biomolecules (Kadiyala et al., 2018). Although the solubility of ZnO in water is small ($K_{\text{sp}} 3.7 \times 10^{-17}$), a trace amount of Zn^{2+} is enough to retard bacteria cell growth. Therefore, the antibacterial activity of $\text{ZnO}_{\text{nano-synth}}\text{-[chi-SiG]}$ is higher than $\text{Zn}_{\text{salt}}\text{-[chi-SiG]}$ against Gram-positive and Gram-negative bacteria, although Zn^{2+} from $\text{Zn}_{\text{salt}}\text{-[chi-SiG]}$ is more mobile than from ZnO . This finding confirmed the antimicrobial ZnO either

alone or with other metal oxides as previously reported in the literature although with different preparation methods (Alabyadh et al., 2022; Yazdi et al., 2021; Mousavi-Kouhi, 2021).

All experiments were performed in triplicates and reported as mean \pm standard deviation (SD).

3.4. Antibacterial studies of air filter assembled immobilized ZnO

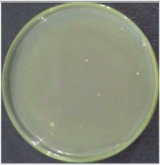
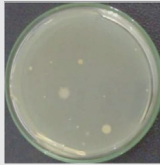
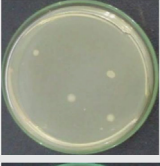
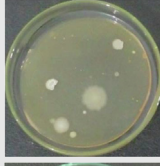
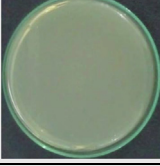
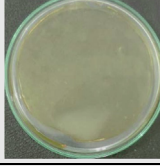
Each granule of $\text{ZnO}_{\text{nano-synth}}\text{-[chi-SiG]}$, $\text{Zn}_{\text{salt}}\text{-[chi-SiG]}$, chi-SiG, and SiG was assembled as an air filter panel (Fig. 3) and inserted into the air filter chamber (Fig. 2). The HEPA filter bacterial activity was also compared to $\text{ZnO}_{\text{nano-synth}}\text{-[chi-SiG]}$ filter efficacy. Since the dominant bacteria were *Bacillus sp.* in the indoor air (Harbizadeh et al., 2019), therefore the experiment was limited to *Bacillus subtilis* which can produce spores in relatively dry conditions. In the air filter chamber, an agar petri dish containing *B. subtilis* was blown by a small fan, and then when the humidity slowly decreased, thus *B. subtilis* became stressed and produced endospores (Higgins & Dworkin, 2012) that would be flown to penetrate the filter.

The number of bacteria colonies before and after contacting the filter was compared as presented in Table 7 and some

Table 7 Observation results of colonies using a colony counter for the filters.

Filter	Initial colonies before filter penetration	Incubation time (h)	The survival colonies after penetration	Inactivation rate (%)
No filter	330	24	24	Control
		48	26	
SiG	336	24	9	63
		48	26	0
HEPA filter cloth	342	24	19	21
		48	24	8
chi-SiG	339	24	0	100
		48	6	69
$\text{Zn}_{\text{salt}}\text{-[chi-SiG]}$	340	24	4	83
		48	5	81
$\text{ZnO}_{\text{nano-synth}}\text{-[chi-SiG]}$	342	24	2	92
		48	2	92

Table 8 Colonies observation after through the filters.

Filter	Incubation time (24 h)	Incubation time (48 h)
SiG		
HEPA filter cloth		
ZnO _{nano-synth} -[chi-SiG]		

representative colony images are shown in Table 8. The counted colonies in 24 and 48 h observations were displayed in Table 7. The number of bacterial colonies in the air before passing through the filter was 330–342 colonies. The number of colonies was extremely smaller in the area shared by the filter because not all bacteria were flown to penetrate the filter. The flown bacteria in control (without filter) was only 24–26 colonies observed in 24 and 48 h. The colonies were considered as the maximum survival colonies (control) flown toward the filter in 24 h (24 colonies) and 48 h incubation (26 colonies) that were used for the calculation of the inactivation rate of filters. The ZnO_{nano-synth}-[chi-SiG] filter performed the highest antibacterial property compared to other filters except for chi-SiG. Although chi-SiG seems to show the highest antibacterial activity it was in only a short time (24 h), then the bacteria grew after 48 h. The ZnO_{nano-synth}-[chi-SiG] filter retard colony growth into 2 colonies (92% efficacy) in 24 and 48 h. If it is compared to the initial colonies which were 342, then the survival was only 2 colonies in 24 and 48 h, then the inactivation rate would be 99% efficacy for the ZnO_{nano-synth}-[chi-SiG] filter. This finding confirmed might relate to ZnO_{nano-synth} particle size that has a high surface-to-volume ratio leading to improve antibacterial activity against bacteria and spores. The data are consistent with the above ZnO-type characteristics.

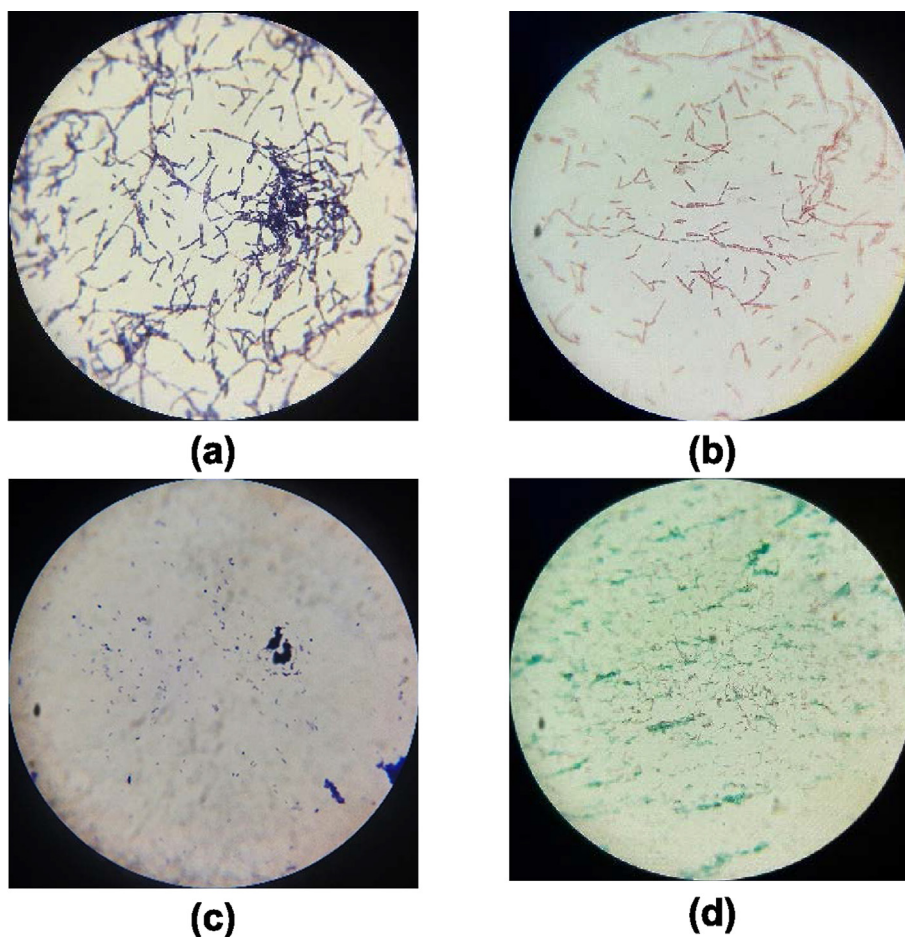


Fig. 12 Microscopic images of *B. subtilis* (a) Gram staining after through SiG filter, (b) spore staining after through SiG filter, (c) Gram staining after through ZnO_{nano-synth}-[chi-SiG] filter, and (d) spore staining after through ZnO_{nano-synth}-[chi-SiG] filter with 1000 × magnification.

These results confirmed that both chitosan and zinc ions showed moderate antibacterial activity, but the chitosan-only filter showed that the colonies continue growth after 24 h. It is proven that a filter containing ZnO_{nano-synth}-[chi-SiG] prevents air contamination in prolonged activity.

To compare the existence of bacteria after penetration of air SiG filter (control) and after contact or penetration with ZnO_{nano-synth}-[chi-SiG] filter was also studied. After penetration SiG, many bacteria were still alive and had coccus or basil shapes (Fig. 12a). The spores staining found that spores and vegetative cells still exist, indicating the alive cells and metabolically active (Fig. 12b). It was very different after bacteria penetrate ZnO_{nano-synth}-[chi-SiG] filter, the spore, and Gram staining show the cells were shrunk and had an irregular shape and unusual color (Fig. 12c). The spores were not found inside the vegetative cells (Fig. 12d). Therefore, the existence of ZnO_{nano-synth} with air filter is confirmed to stop the sporulation process and significantly modify metabolism in *B. subtilis* (Rosi & Mirkin, 2005; Eymard-Vernain et al., 2018). The findings are also consistent with the previous studies on *B. subtilis* that showed ZnO nanoparticles initiate the sporulation and inhibit the cell growth of *B. subtilis* bacteria (Godoy-Gallardo et al., 2021; Hsueh et al., 2015; Matyszczyk & Krzepilko, 2022).

However, ZnO nanoparticles selectively harm bacteria while having little effect on human and animal tissues. Zinc is recognized as an essential trace element for the physiological and biochemical processes in humans and animals (Baek & An, 2011). Therefore, the Food and Drug Administration (FDA) considered ZnO as a generally recognized safe substance (GRAS). The GRAS designation mostly encompasses materials ranging from microns to larger sizes so, conversion of these macro substances to nanoscale will attain distinctive properties including toxicity.

ZnO bactericidal performance in this current study is aligned with the previous studies proving ZnO to retard cancer cell growth in vitro of human liver hepatocellular carcinoma (HepG2) (Tanino et al., 2020). ZnO nanoparticles can activate ROS fabrication in cancer cells and ultimately destroy the cancer cell which consequently leads to cancer cell death (Yazdi et al., 2021). Cancer cells are different from normal cells, especially in terms of metabolic requirements; this leads to different cytotoxicity results (Rajendran et al., 2017). The cytotoxicity effect of ZnO nanoparticles against a normal cell revealed less toxicity than a cancerous cell (Yadav et al., 2022; Mousavi-Kouhi et al., 2021; Yazdi et al., 2021; Alabyadh et al., 2022).

4. Conclusion

Synthesis and immobilization of ZnO_{nano-synth} on white silica gel beads coated with chitosan were proved to be a low-cost and environmentally friendly procedure with high antibacterial properties. After testing several solvents, methanol-sodium hydroxide was confirmed as the proper reagent for the preparation and immobilization of ZnO_{nano-synth} onto chi-SiG. Subsequently, the drying process at 60 °C for 72 h affected the dispersed and nanoparticle size of ZnO. The chitosan coat was proved to act as the stabilizer and the adhesive for ZnO_{nano-synth} on the white silica gel beads surface. The ZnO_{nano-synth}-[chi-SiG] which has dispersed small nanoparticle size, exhibited the strongest antibacterial activity against Gram-positive and Gram-negative bacteria in agar media, if it is compared to the ZnO commercial nanopowder, and the Zn precursor bacterial activities. The air filter containing ZnO_{nano-synth}-[chi-SiG] showed high antibacterial performance against *B. subtilis* in the air.

Declaration of Competing Interest

The authors declare that they have no known competing financial interests or personal relationships that could have appeared to influence the work reported in this paper.

Acknowledgment

This work was supported by the PMDSU Scholarship for Muhammad Iqbal Hidayat and a Research fund from The Ministry of Education, Culture, Research, and Technology, Republic of Indonesia (grant number 060/E5/PG.02.00.PT/2022); and PKPI PMDSU (grant number 085.36/E4.4/KU/2022). Part of this work was also supported by the bridging grant (304/PKIMIA/6316598) from Universiti Sain Malaysia.

References

- Adlim, M., Bakar, M.A., 2013. The properties of Pd/Au bimetallic colloidal catalysts stabilized by chitosan and prepared by simultaneous and stepwise chemical reduction of the precursor ions. *Kinet. Catal.* 54, 586–596. <https://doi.org/10.1016/j.jbiomac.2019.04.196>.
- Adlim, M., Hidayat, M.I., Azmi, N., Ramayani, R.F.I., 2021. Preparation of chitosan-silver nanoparticles immobilized onto pumice for antibacterial testing against *Escherichia coli*. *Proceedings of the 2nd ICECME, Banda Aceh, Indonesia*. p. 63-72. 10.1007/978-981-16-0736-3_7.
- Adlim, M., Zarlaida, F., Rahmayani, R.F.I., Wardani, R., 2019. Nutrient release properties of a urea-magnesium-natural rubber composite coated with chitosan. *Environ. Technol. Innov.* 16. <https://doi.org/10.1016/j.eti.2019.100442> 100442.
- Adlim., Bakar, M.A., 2008. Preparation of chitosan-gold nanoparticles: part 2 (finish). The role of chitosan. *Indo. J. Chem.* 8(3), 320-326. 10.22146/ijc.21585.
- Ahmad, I., Akhtar, M.S., Manzoor, M.F., Wajid, M., Noman, M., Ahmed, E., Ahmad, M., Khan, W.Q., Rana, A.M., 2021. Synthesis of yttrium and cerium doped ZnO nanoparticles as highly inexpensive and stable photocatalysts for hydrogen evolution. *J. Rare Earths* 39 (4), 440–445. <https://doi.org/10.1016/j.jre.2020.04.002>.
- Alabyadh, T., Albadri, R., Es-haghi, A., Yazdi, M.E.T., Ajalli, N., Rahdar, A., Thakur, V.K., 2022. ZnO/CeO₂ nanocomposites: metal-organic framework-mediated synthesis, characterization, and estimation of cellular toxicity toward liver cancer cells. *J. Funct. Biomater.* 13, 139. <https://doi.org/10.3390/jfb13030139>.
- Ali, A., Pan, M., Tilly, T.B., Zia, M., Wu, C.Y., 2018. Performance of silver, zinc, and iron nanoparticles-doped cotton fibers against airborne *E. coli* to minimize bioaerosol exposure. *Air Qual. Atmos. Health* 11, 1233–1242. <https://doi.org/10.1007/s11869-018-0622-0>.
- Aljabali, A.A.A., Akkam, Y., Al Zoubi, M.S., Al-Batayneh, K.M., Al-Trad, B., Alrob, O.A., Alkilany, A.M., Benamara, M., Evan, D.J., 2018. Synthesis of gold nanoparticles using leaf extract of *Ziziphus zizyphus* and their antimicrobial activity. *Nanomaterials (Basel)* 8 (3), 1–5. <https://doi.org/10.3390/nano8030174>.
- Amininezhad, S.M., Amininejad, S.M., Eslamian, S., 2014. Disinfection of Water and Nanotechnology, in *Handbook of Engineering Hydrology*, Ch. 3, Vol. 3: Environmental Hydrology and Water Management, Ed. By Eslamian, S., Taylor and Francis, CRC Group, USA, 51-64.
- Arakha, M., Saleem, M., Mallick, B.C., Jha, S., 2015. The effects of interfacial potential on antimicrobial propensity of ZnO nanoparticle. *Sci. Rep.* 5, 9578. <https://doi.org/10.1038/srep09578>.
- Ardean, C., Davidescu, C.M., Nemeş, N.S., Negrea, A., Ciopec, M., Duteanu, N., Negrea, P., Duda-Seiman, D., Musta, V., 2021.

- Factors influencing the antibacterial activity of chitosan and chitosan modify by functionalization. *Int. J. Mol. Sci.* 22 (14), 7449. <https://doi.org/10.3390/ijms22147449>.
- Baek, Y.W., An, Y.J., 2011. Microbial toxicity of metal oxide nanoparticles (CuO, NiO, ZnO, and Sb₂O₃) to *Escherichia coli*, *Bacillus subtilis*, and *Streptococcus aureus*. *Sci. Total Environ.* 409 (8), 1603–1608. <https://doi.org/10.1016/j.scitotenv.2011.01.014>.
- Balogun, S.W., James, O.O., Sanusi, Y.K., Olayinka, O.H., 2020. Green synthesis and characterization of zinc oxide nanoparticles using bashful (*Mimosa pudica*), leaf extract: a precursor for organic electronics applications. *SN Appl. Sci.* 2, 504. <https://doi.org/10.1007/s42452-020-2127-3>.
- Bankar, D.B., Kanade, K.G., Hawaldar, R.R., Arbuji, S.S., Shinde, M. D., Takle, S.P., Amalnerkar, D.P., Shinde, S.T., 2020. Facile synthesis of nanostructured Ni-Co/ZnO material: an efficient and inexpensive catalyst for Heck reactions under ligand-free conditions. *Arab. J. Chem.* 13, 9005–9018. <https://doi.org/10.1016/j.arabjc.2020.10.023>.
- Bindu, P., Thomas, S., 2014. Estimation of lattice strain in ZnO nanoparticles: X-ray peak profile analysis. *J. Theor. Appl. Phys.* 8, 123–134. <https://doi.org/10.1007/s40094-014-0141-9>.
- Biron, D.D.S., Santos, V.D., Bergmann, C.P., 2020. Synthesis and characterization of the zinc oxide obtained by combining zinc nitrate with sodium hydroxide in polyol medium. *Mater. Res.* 23 (2), e20200080.
- Bose, J.L., Bayles, K.W., 2013. *Staphylococcus aureus*. University of Nebraska Medical Center, Omaha.
- Ciorîță, A., Suciuc, M., Coroș, M., Varodi, C., Pogăcean, F., Măgerușan, L., Mirel, V., Ștefan-van Staden, R.-I., Pruneanu, S., 2023. Antibacterial enhancement of high-efficiency particulate air filters modified with graphene-silver hybrid material. *Microorganisms* 11, 74. <https://doi.org/10.3390/microorganisms11030745>.
- Costa-Pinto, A.R., Lemos, A.L., Tavaría, F.K., Pintado, M., 2021. Chitosan and hydroxyapatite based biomaterials to circumvent periprosthetic joint infections. *Materials* 14 (4), 804. <https://doi.org/10.3390/ma14040804>.
- De Almeida, D.S., Martins, L.D., Aguiar, M.L., 2022. Air pollution control for indoor environments using nanofiber filters: A brief review and post-pandemic perspectives. *Chem. Eng. J. Adv.* 11, <https://doi.org/10.1016/j.cej.2022.100330> 100330.
- Decelis, S., Sardella, D., Triganza, T., Brincat, J.P., Gatt, R., Valdramidis, V.P., 2017. Assessing the anti-fungal efficiency of filters coated with zinc oxide nanoparticles. *R. Soc. Open Sci.* 4, <https://doi.org/10.1098/rsos.161032> 161032.
- Deng, X., Luan, Q., Chen, W., Wang, Y., Wu, M., Zhang, H., Jiao, Z., 2009. Nanosized zinc oxide particles induce neural stem cell apoptosis. *Nanotechnology* 20, (11). <https://doi.org/10.1088/0957-4484/20/11/115101> 115101.
- Donia, D.T., Bauer, E.M., Missori, M., Roselli, L., Cecchetti, D., Tagliatesta, P., Gontrani, L., Carbone, M., 2021. Room temperature syntheses of ZnO and their structures. *Symmetry* 13 (4), 733. <https://doi.org/10.3390/sym13040733>.
- Duan, C., Meng, X., Meng, J., Khan, M.I.H., Dai, L., Khan, A., An, X., Zhang, J., Huq, T., Ni, Y., 2019. Chitosan as a preservative for fruits and vegetables: a review on chemistry and antimicrobial properties. *J. Bioresour. Bioprod.* 4 (1), 11–21. <https://doi.org/10.21967/jbb.v4i1.189>.
- Dubey, S., Rohra, H., Taneja, A., 2021. Assessing effectiveness of air purifiers (HEPA) for controlling indoor particulate pollution. *Heliyon* 7 (9), e07976.
- Eymard-Vernain, E., Coute, Y., Adrait, A., Rabilloud, T., Sarret, G., Lelong, C., 2018. The polygamma-glutamate of *Bacillus subtilis* interacts specifically with silver nanoparticles. *PLoS ONE* 13 (5), 1–19. <https://doi.org/10.1371/journal.pone.0197501>.
- Faisal, S., Jan, H., Shah, S.A., Shah, S., Khan, A., Akbar, M.T., Rizwan, M., Jan, F., Akhtar, N., Khattak, A., Syed, S., 2021. Green synthesis of zinc oxide (ZnO) nanoparticles using aqueous fruit extracts of *myristica fragrans*: their characterizations and biological and environmental applications. *ACS Omega* 6 (14), 9709–19022. <https://doi.org/10.1021/acsomega.1c00310>.
- Forthomme, A., Joubert, A., Andrès, Y., Simon, X., Duquenne, P., Bemer, D., Coq, L.L., 2014. Microbial aerosol filtration: growth and release of a bacteria–fungi consortium collected by fibrous filters in different operating conditions. *J. Aerosol Sci.* 72, 32–46. <https://doi.org/10.1016/j.jaerosci.2014.02.004>.
- Gerhardt, P., 1980. *Manual of methods for general bacteriology*. Am. Soc. Microbiol.
- Godoy-Gallardo, M., Eckhard, U., Delgado, L.M., de Roo Puente, Y. J.D., Hoyos-Nogués, M., Gil, F.J., Perez, R.A., 2021. Antibacterial approaches in tissue engineering using metal ions and nanoparticles: from mechanisms to applications. *Bioact. Mater.* 6 (12), 4470–4790. <https://doi.org/10.1016/j.bioactmat.2021.04.033>.
- Govindarajan, D.K., Viswalingam, N., Meganathan, Y., Kandaswamy, K., 2020. Adherence patterns of *Escherichia coli* in the intestine and its role in pathogenesis. *Medicine in Microecology* 5, <https://doi.org/10.1016/j.medmic.2020.100025> 100025.
- Gudkov, S.V., Burmistrov, D.E., Serov, D.A., Rebezov, M.B., Semenova, A.A., Lisitsyn, A.B., 2021. A mini review of antibacterial properties of ZnO nanoparticles. *Front. Phys.* 9, <https://doi.org/10.3389/fphy.2021.641481> 641481.
- Haase, M., Weller, H., Henglein, A., 1988. Photochemistry and radiation chemistry of colloidal semiconductors 23 electron storage on zinc oxide particles and size quantization. *J. Phys. Chem.* 92 (2), 482–487. <https://doi.org/10.1021/j100313a047>.
- Han, M.C., He, H.W., Kong, W.K., Dong, K., Wang, B.Y., Yan, X., Wang, L.M., Ning, X., 2022. High-performance electret and antibacterial polypropylene meltblown nonwoven materials doped with Boehmite and ZnO nanoparticles for air filtration. *Fibers Polym.* 23, 1947–1955. <https://doi.org/10.1007/s12221-022-4786-8>.
- Harbizadeh, A., Mirzaee, S.A., Khosravi, A.D., Shoushtari, F.S., Goodarzi, H., Alavi, N., Ankali, K.A., Dad, H.D., Maleki, H., Goodarzi, G., 2019. Indoor and outdoor airborne bacterial air quality in day-care centers (DCCs) in greater Ahvaz. *Iran. Atmos. Environ.* 216, <https://doi.org/10.1016/j.atmosenv.2019.116927> 116927.
- Headd, B., Bradford, S.A., 2016. Use of aerobic spores as a surrogate for cryptosporidium oocysts in drinking water supplies. *Water Res.* 90, 185–202. <https://doi.org/10.1016/j.watres.2015.12.024>.
- Hidayat, M.I., Adlim, M., Maulana, I., Zulfajri, M., 2021. Immobilization of silver nanoparticles on chitosan-coated silica-gel-beads and the antibacterial activity. *Key Eng. Mater.* 892, 36–42. <https://doi.org/10.4028/www.scientific.net/KEM.892.36>.
- Hidayat, M.I., Adlim, M., Maulana, I., Suhartono, S., Hayati, Z., Bakar, N.H.H.A., 2022. Green synthesis of chitosan-stabilized silver-colloidal nanoparticles immobilized on white-silica-gel beads and the antibacterial activities in a simulated-air-filter. *Arab. J. Chem.* 15, (2). <https://doi.org/10.1016/j.arabjc.2021.103596> 103596.
- Higgins, D., Dworkin, J., 2012. Recent progress in *Bacillus subtilis* sporulation. *FEMS Microbiol. Rev.* 36 (1), 131–148. <https://doi.org/10.1111/j.1574-6976.2011.00310.x>.
- Hsueh, Y.H., Ke, W.J., Hsieh, C.T., Lin, K.S., Tzou, D.Y., Chiang, C. L., 2015. ZnO nanoparticles affect *Bacillus subtilis* cell growth and biofilm formation. *PLoS ONE* 10 (6), e0128457.
- Huang, W., Tao, F., Li, F., Mortimer, M., Guo, L.H., 2020. Antibacterial nanomaterials for environmental and consumer product applications. *Nanoimpact* 20, <https://doi.org/10.1016/j.impact.2020.100268> 100268.
- Hussey, M.A., Zayaitz, A., 2007. Endospore stain protocol. *Am. Soc. Microbiol.* 8.
- Jafarirad, S., Mehrabi, M., Divband, B., Kosari-Nasab, M., 2016. Biofabrication of zinc oxide nanoparticles using fruit extract of *Rosa canina* and their toxic potential against bacteria: a mechanistic approach. *Mater. Sci. Eng. C* 59, 296–302. <https://doi.org/10.1016/j.msec.2015.09.089>.
- Jatoi, A.W., Kim, I.S., Ogasawara, H., Ni, Q.-Q., 2019. Characterization and application of CA/ZnO/AgNP composite nanofibers

- for sustained antibacterial properties. *Mater. Sci. Eng. C* 105, <https://doi.org/10.1016/j.msec.2019.110077> 110077.
- Kadiyala, U., Tulari-Emre, E.S., Bahng, J.H., Kotov, N.A., VanEpps, J.S., 2018. Unexpected insights into antibacterial activity of zinc oxide nanoparticles against methicillin resistant: *Staphylococcus aureus* (MRSA). *Nanoscale* 10 (10), 4927–4939. <https://doi.org/10.1039/c7nr08499d>.
- Kanchana, S., Chithra, M.J., Ernest, S., Pushpanathan, K., 2016. Violet emission from Fe doped ZnO nanoparticles synthesized by precipitation method. *J. Lumin.* 176, 6–14. <https://doi.org/10.1016/j.jlumin.2015.12.047>.
- Khoshhesab, Z.M., Sarfaraz, M., Asadabad, M.A., 2011. Precipitation of ZnO nanostructures by chemical precipitation method. *Synth. React. Inorg. Met. Org. Nano-Met. Chem.* 41 (7), 814–819. <https://doi.org/10.1080/15533174.2011.591308>.
- Kulawik, P., Jamróz, E., Özogul, F., 2020. Chitosan role for shelf-life extension of seafood. *Environ. Chem. Lett.* 18, 61–74. <https://doi.org/10.1007/s10311-019-00935-4>.
- Kumar, S., Krishnakumar, B., Sobral, A.J.F.N., Koh, J., 2019. Bio-based (chitosan/PVA/ZnO) nanocomposites film: thermally stable and photoluminescence material for removal of organic dye. *Carbohydr. Polym.* 205, 559–564. <https://doi.org/10.1016/j.carbpol.2018.10.108>.
- Li, Y., Miao, Q., Wang, X., 2022. Antibacterial capability of air filter fiber materials treated with triclosan against indoor environmental microbes. *Atmosphere* 13, 1104. <https://doi.org/10.3390/atmos13071104>.
- Li, X., Weng, Z., Cao, A., Liu, Q., Sui, G., 2018. An overview about varieties and detection methods of pathogenic microorganisms in indoor air. *Chin. Sci. Bull.* 63 (21), 2116–2127. <https://doi.org/10.1360/N972018-00328>.
- Lowther, S.D., Deng, W., Fang, Z., Booker, D., Whyatt, D.J., Wild, O., Wang, X., Jones, K.C., 2020. How efficiently can HEPA purifiers remove priority fine and ultrafine particles from indoor air? *Environ. Int.* 144, <https://doi.org/10.1016/j.envint.2020.106001> 106001.
- Matyszczuk, K., Krzepilko, A., 2022. Model study for interaction of sublethal doses of zinc oxide nanoparticles with environmentally beneficial bacteria *Bacillus thuringiensis* and *Bacillus megaterium*. *Int. J. Mol. Sci.* 23 (19), 11820. <https://doi.org/10.3390/ijms231911820>.
- Mousavi-Kouhi, S.M., Beyk-Khormizi, A., Amiri, M.S., Mashreghi, M., Yazdi, M.E.T., 2021. Silver-zinc oxide nanocomposite: from synthesis to antimicrobial and anticancer properties. *Ceram. Int.* 47, 21490–21497. <https://doi.org/10.1016/j.ceramint.2021.04.160>.
- Muktaridha, O., Adlim, M., Suhendrayatna, S., Ismail, I., 2021. Progress of 3d metal-doped zinc oxide nanoparticles and the photocatalytic properties. *Arab. J. Chem.* 14, (6). <https://doi.org/10.1016/j.arabjc.2021.103175> 103175.
- Muktaridha, O., Adlim, M., Suhendrayatna, S., Ismail, I., 2022. Highly reusable chitosan-stabilized Fe-ZnO immobilized onto fiberglass cloth and the photocatalytic degradation properties in batch and loop reactors. *J. Saudi Chem. Soc.* 26, (3). <https://doi.org/10.1016/j.jscs.2022.101452> 101452.
- Nunes, S.P., Culfaz-Emecen, P.Z., Ramon, G.Z., Visser, T., Koops, G. H., Jin, W., Ulbricht, M., 2020. Thinking the future of membranes: perspectives for advanced and new membrane materials and manufacturing processes. *J. Membr. Sci.* 598, <https://doi.org/10.1016/j.memsci.2019.117761> 117761.
- PubChem, 2005. Compound summary of sodium hydroxide. <https://pubchem.ncbi.nlm.nih.gov/compound/Sodium-hydroxide> (accessed 26 January 2023).
- Rajendra, K., Sen, S., Suja, G., Senthil, S.L., Kumar, T.V., 2017. Evaluation of cytotoxicity of hematite nanoparticles in bacteria and human cell lines. *Colloids Surf. B Biointerfaces* 157, 101–109. <https://doi.org/10.1016/j.colsurfb.2017.05.052>.
- Ranjani, B., Pandian, K., Kumar, G.A., Gopinath, S.C.B., 2019. D-glucosamine chitosan base molecule-assisted synthesis of different shape and sized silver nanoparticles by a single pot method: A greener approach for sensor and microbial applications. *Int. J. Biol. Macromol.* 133, 1280–1287. <https://doi.org/10.1016/j.ijbiomac.2019.04.196>.
- Rosi, N.L., Mirkin, C.A., 2005. Nanostructures in biodiagnostics. *Chem. Rev.* 105 (4), 1547–1562. <https://doi.org/10.1021/cr030067f>.
- Sarojini, S.K., Indumathi, M.P., Rajarajeswari, G.R., 2019. Mahua oil-based polyurethane/chitosan/nano ZnO composite films for biodegradable food packaging applications. *Int. J. Biol. Macromol.* 124, 163–174. <https://doi.org/10.1016/j.ijbiomac.2018.11.195>.
- Setlow, P., 2006. Spores of *Bacillus subtilis*: their resistance to and killing by radiation, heat and chemicals. *J. App. Microbiol.* 101 (3), 514–525. <https://doi.org/10.1111/j.1365-2672.2005.02736.x>.
- Sigma Aldrich, 2023a. Gold(III) chloride solution 99.99% trace metals basis. <https://www.sigmaaldrich.com/ID/en/product/aldrich/484385> (accessed 15 April 2023).
- Sigma Aldrich, 2023b. Silver nitrate 99.99% trace metals basis. <https://www.sigmaaldrich.com/ID/en/product/aldrich/204390> (accessed 15 April 2023).
- Sigma Aldrich, 2023c. Zinc nitrate hydrate 99.99% trace metals basis. <https://www.sigmaaldrich.com/ID/en/product/aldrich/230006> (accessed 15 April 2023).
- Silica-Gel Desiccants, 2023. Silica gel white beads & crystals. <https://www.silicagel-desiccant.com/silica-gel-white> (accessed 5 January 2023).
- Siripatrawan, U., Vitthayakitti, W., 2016. Improving functional properties of chitosan films as active food packaging by incorporating with propolis. *Food Hydrocoll.* 61, 695–702. <https://doi.org/10.1016/j.foodhyd.2016.06.001>.
- Soon, C.Y., Tee, Y.B., Tan, C.H., Rosnita, A.T., Khalina, A., 2018. Extraction and physicochemical characterization of chitin and chitosan from *Zophobas morio* larvae in varying sodium hydroxide concentration. *Int. J. Biol. Macromol.* 108, 135–142. <https://doi.org/10.1016/j.ijbiomac.2017.11.138>.
- Sun, J., Jiang, H., Wu, H., Tong, C., Pang, J., Wu, C., 2020. Multifunctional bionanocomposite films based on konjac glucomannan/chitosan with nano-ZnO and mulberry anthocyanin for active food packaging. *Food Hydrocoll.* 107, <https://doi.org/10.1016/j.foodhyd.2020.105942> 105942.
- Tadji, A., Abderrahmane, A., Zerdali, M., Hamzaoui, S., 2022. Facile preparation of nanostructured ZnO via low-temperature hydrothermal method upon changing the precursor anion: the study of structural, morphological, and optical properties. *Mater. Today Chem.* 31, <https://doi.org/10.1016/j.mtcomm.2022.103789> 103789.
- Tanino, R., Amano, Y., Tong, X., Sun, R., Tsubata, Y., Harada, M., Fujita, Y., Isobe, T., 2020. Anticancer activity of ZnO nanoparticles against human small-cell lung cancer in an orthopaedic mouse model. *Mol. Cancer Ther.* 19 (2), 502–512. <https://doi.org/10.1158/1535-7163.MCT-19-0018>.
- Vijayalakshmi, U., Chellappa, M., Anjaneyulu, U., Manivasagam, G., Sethu, S., 2015. Influence of coating parameter and sintering atmosphere on the corrosion resistance behavior of electrophoretically deposited composite coatings. *Mater. Manuf. Process* 31 (6), 95–106. <https://doi.org/10.1080/10426914.2015.1070424>.
- Vu, T.V., Stewart, G.B., Kitwiroon, N., Lim, S., Barratt, B., Kelly, F. J., Thompson, R., Smith, R.B., Toledano, M.B., Beevers, S.D., 2022. Assessing the contributions of outdoor and indoor source to air quality in London homes of the SCAMP cohort. *Build. Environ.* 222, <https://doi.org/10.1016/j.buildenv.2022.109359> 109359.
- Watson, R., Oldfield, M., Bryant, J.A., Riordan, L., Hill, H.J., Watts, J.A., Alexander, M.R., Cox, M.J., Stamatakis, Z., Scurr, D.J., Cogan, F.D., 2022. Efficacy of antimicrobial and anti-viral coated air filters to prevent the spread of airborne pathogens. *Sci. Rep.* 12, 2803. <https://doi.org/10.1038/s41598-022-06579-9>.
- Wightman, P.G., Fein, J.B., Wesolowski, D.J., Phelps, T.J., Bénézet, P., Palmer, D.A., 2011. Measurement of bacterial surface proto-

- nation constants for two species at elevated temperatures. *Geochim Cosmochim Acta* 65 (21), 3657–3669. [https://doi.org/10.1016/S0016-7037\(01\)00763-3](https://doi.org/10.1016/S0016-7037(01)00763-3).
- Wu, Z., Huang, X., Li, Y.C., Xiao, H., Wang, X., 2018. Novel chitosan films with laponite immobilized Ag nanoparticles for active food packaging. *Carbohydr. Polym.* 199, 210–218. <https://doi.org/10.1016/j.carbpol.2018.07.030>.
- Xiong, M., Wang, C.X., Shao, D.D., 2014. Preparing sodium methoxide from sodium hydroxide by reaction coupling with separation processes. *Adv. Mater. Res.* 986–987, 101–105. <https://doi.org/10.4028/www.scientific.net/AMR.986-987.101>.
- Yadav, S., Sadique, M.A., Pal, M., Khan, R., Srivastava, A.K., 2022. Cytotoxicity and DNA fragmentation-mediated apoptosis response of hexagonal ZnO nanorods against human prostate cancer cells. *Appl. Surf. Sci. Adv.* 9, <https://doi.org/10.1016/j.ap-sadv.2022.100237> 100237.
- Yang, H., Liu, C., Yang, D., Zhang, H., Xi, Z., 2009. Comparative study of cytotoxicity, oxidative stress and genotoxicity induced by four typical nanomaterials: the role of particle size, shape, and composition. *J. Appl. Toxicol.* 29 (1), 69–78. <https://doi.org/10.1002/jat.1385>.
- Yao, Z., Xia, M., Xiong, Z., Wu, Y., Cheng, P., Cheng, Q., Xu, J., Wang, D., Liu, K., 2022. A hierarchical structure of flower-like zinc oxide and poly(vinyl alcohol-co-ethylene) nanofiber hybrid membranes for high-performance air filters. *ACS Omega* 7 (3), 3030–3036. <https://doi.org/10.1021/acsomega.1c06114>.
- Yazdi, M.E.T., Nourbakhsh, Mashreghi, M., Mousavi, S.H., 2021. Ultrasound-based synthesis of ZnO.Ag₂O₃ nanocomposite: characterization and evaluation of its antimicrobial and anticancer properties. *Res. Chem. Intermed.* 47, 1285–1296. <https://doi.org/10.1007/s11164-020-04355-w>.
- Zarharan, H., Bagherian, M., Rokhi, A.S., Bajgiran, R.R., Yousefi, E., Heravian, P., Khazrabig, M.N., Es-haghi, A., Yazdi, M.E.T., 2023. The anti-angiogenesis and antioxidant activity of chitosan-mediated synthesized selenium-gold nanostructure. *Arab. J. Chem.* 16, <https://doi.org/10.1016/j.arabjc.2023.104806> 104806.
- Zhai, F., Luo, Y., Zhang, Y., Liao, S., Cheng, J., Meng, X., Zeng, Y., Wang, X., Yang, J., Yin, J., Li, L., 2022. Viscosity simulation of glass microfiber and an unusual air filter with high-efficiency antibacterial functionality enabled by ZnO/graphene-modified glass microfiber. *ACS Omega* 7 (16), 14211–14221. <https://doi.org/10.1021/acsomega.2c00838>.
- Zhang, W., Deng, S., Zhang, S., Yang, Z., Lin, Z., 2022. Energy consumption performance optimization of PTFE HEPA filter media during dust loading through compositing them with the efficient filter medium. *Sustain. Cities Soc.* 78, <https://doi.org/10.1016/j.scs.2021.103657> 103657.
- Zhong, Z., Xu, Z., Sheng, T., Yao, J., Xing, W., Wang, Y., 2015. Unusual air filters with ultrahigh efficiency and antibacterial functionality enabled by ZnO nanorods. *ACS Appl. Mater. Interfaces* 7 (38), 21538–21544. <https://doi.org/10.1021/acsomega.5b06810>.